JOURNAL OF GEOPHYSICAL RESEARCH, VOL. 113, B03305, doi:10.1029/2007JB004950, 2008

Click Here for Full Article

Regional seismic observations of the 9 October 2006 underground nuclear explosion in North Korea and the influence of crustal structure on regional phases

Tae-Kyung Hong,[1] Chang-Eob Baag,[2] Hoseon Choi,[2,3] and Dong-Hoon Sheen[2,4,5]

Received 23 January 2007; revised 31 October 2007; accepted 26 December 2007; published 15 March 2008.

[1] The crustally guided shear wave, *Lg*, is typically the most prominent phase of a nuclear explosion at regional distance. This *Lg* phase is analyzed often to discriminate a nuclear explosion from a natural earthquake. In addition, the *Lg* phase allows us to determine the size of the detonation. A nuclear explosion test in North Korea was conducted on 9 October 2006. The epicenter was located close to the eastern shore of the Korean Peninsula, resulting in raypaths that vary significantly according to the azimuths. In particular, rays radiated in the southern direction experience lateral variation of crustal structures at the continental margin. We examine the influence of raypaths on regional seismic phases by comparing the spectra and waveforms from different raypaths. Three natural earthquakes in North Korea are also examined to determine the raypath effect. We find that the *Lg* from the nuclear explosion dissipated significantly as result of energy leakage into the mantle resulting from variations in crustal thickness along the portion of the raypath traversing the western tip of the Sea of Japan (East Sea). Some of the leaked energy develops into mantle lid waves (*Sn*), causing a large energy increase to *Sn*. A similar feature is observed in the records of natural earthquakes. This feature is confirmed by seismic waveform modeling. The raypath effect also causes underestimation of magnitude. The *Lg* body wave magnitude, $m_b(Lg)$, is estimated to be 3.8–4.2 for records from pure continental paths and 2.6–3.4 for records from paths crossing continental margins. This result illustrates the need to consider raypath effects for the correct estimation of magnitudes of regional events, including a nuclear explosion.

Citation: Hong, T.-K., C.-E. Baag, H. Choi, and D.-H. Sheen (2008), Regional seismic observations of the 9 October 2006 underground nuclear explosion in North Korea and the influence of crustal structure on regional phases, *J. Geophys. Res.*, *113*, B03305, doi:10.1029/2007JB004950.

1. Introduction

[2] The crustally guided shear wave, *Lg*, is typically the most prominent seismic phase on regional seismograms for both natural earthquakes and nuclear explosions. The strong excitation of regional shear waves from nuclear explosions often makes it difficult to distinguish seismic records of a nuclear explosion from those of earthquakes at low frequency without sophisticated analysis of seismic data, such as *P*/*Lg* ratio analysis, which is particularly useful at high frequencies (3–4 Hz) [e.g., *Walter et al.*, 1995; *Taylor*, 1996; *Fisk*, 2006]. Thus understanding the mechanism of shear wave excitation from underground nuclear explosions (UNEs) is a key issue in nuclear seismology. However, many aspects of shear wave excitation from UNEs still remain unclear despite significant advances in the study of plausible mechanisms [e.g., *Massé*, 1981; *Wallace et al.*, 1985; *Day and McLaughlin*, 1991; *Xie and Lay*, 1994; *Patton and Taylor*, 1995]. Furthermore, the rock responses to nuclear explosions, such as rock cracking and cavity coupling, are not well understood. In addition, the influence of the oceanic environment on regional wave development has rarely been investigated, although regional wave attenuation in continental environment has been widely studied [e.g., *Nuttli*, 1981; *Xie and Patton*, 1999].

[3] The recent nuclear explosion test of North Korea on 9 October 2006 has raised a number of issues including: (1) whether the seismic waveforms are similar to previous UNEs in other areas; (2) why the initial magnitude estimate varies so widely; and finally, (3) whether raypaths through the continental margin beneath the Sea of Japan (East Sea), which are the major raypaths from the UNE to the stations in South Korea, impact regional waveforms. The possible raypath effect may be closely related to the other issues and thus is a focus of this study. We compare regional seismic

[1] Department of Earth System Sciences, Yonsei University, Seoul, South Korea.
[2] School of Earth and Environmental Sciences, Seoul National University, Seoul, South Korea.
[3] Korea Institute of Nuclear Safety, Daejeon, South Korea.
[4] National Institute of Meteorological Research, Korea Meteorological Administration, Seoul, South Korea.
[5] Now at Korea Institute of Geoscience and Mineral Resources, Daejeon, South Korea.

Copyright 2008 by the American Geophysical Union.
0148-0227/08/2007JB004950$09.00

waveforms and spectra from different raypaths. We present $m_b(Pn)$ and $m_b(Lg)$ estimates from various raypaths and discuss the influence of raypaths on the development of regional seismic waves.

2. Data and Geology

[4] A UNE test in North Korea was conducted on 9 October 2006. This nuclear explosion test was confirmed later with the detection of xenon, a radioactive element emitted during a nuclear fission reaction, in the air [*Korea Institute of Nuclear Safety*, 2007]. The magnitude of the UNE was reported to be 3.6–4.2, with an apparent disagreement among international institutions (e.g., Korea Institute of Geoscience and Mineral Resources: local magnitude (M_L) of 3.6; U.S. Geological Survey (USGS): body wave magnitude (m_b) of 4.2). Note that the local magnitude, M_L, is based on the maximum amplitude in seismograms, which typically corresponds to the *Lg* amplitude in regional seismograms. The body wave magnitude, m_b, of USGS is based on teleseismic phases, which are rarely influenced by the crustal structure along the raypath.

[5] The nuclear explosion test was well recorded at regional distance seismic stations in the southern Korean Peninsula and neighboring countries. We collect broadband seismic records from stations in South Korea and China (Figure 1). We also examine regional records for three natural earthquakes that occurred in or around North Korea in order to identify the characteristic features of the UNE (Table 1 and Figure 1). The epicentral distances between events and stations range from 370 to 671 km.

[6] The major geological structure of the Korean Peninsula consists of three massifs (Nangrim Massif, Kyonggi Massif, Yongnam Massif) that are separated by intervening tectonic belts (Imjingang Belt, Okchon Belt, etc.) (see Figure 1b) [e.g., *Chough et al.*, 2000; *Sagong et al.*, 2003]. The continental shelf on the western edge of the Sea of Japan (East Sea) composes the continental margin that transforms a normal continental crust to either a rifted continental crust or an oceanic crust [*Chough et al.*, 2000; *Cho et al.*, 2004; *Yu*, 2006]. The lower crust in the continental margin off the southeast of the Korean Peninsula is underplated by intrusive solidated magma, which causes abrupt seismic velocity increases in the lower crust because of the emplacement of dense magmatic materials [*Cho et al.*, 2004].

[7] The Moho depth is shallow in central Korea and relatively deep in southern and northern Korea, with ranges between 28 and 38 km [*Chang and Baag*, 2005; *Yu*, 2006]. The crustal thickness decreases rapidly with distance from the eastern shore of the peninsula toward the Sea of Japan (East Sea) (Figure 1b). The center of Gyeongsang Basin composes the maximum crustal thickness in southern Korea, with a notable high-velocity structure in the lower crust at the southeastern end [*Chang and Baag*, 2005; *Cho et al.*, 2006].

3. Waveform Variation

[8] Regional seismic wavefields from both nuclear explosions and natural earthquakes typically consist of mantle lid head waves (*Pn* and *Sn*), crustally reflected (or guided) waves (*Pg* and *Lg*), and fundamental mode Rayleigh waves (*Rg*) (Figures 2, 3, and 4) [e.g., *Hong and Xie*, 2005]. Since, however, the *Rg* waves from nuclear explosions are typically weaker than those from natural earthquakes [*Patton*, 2001], the regional seismic records for underground nuclear explosions are usually dominated by *Lg*.

[9] The crustal-guided shear waves (*Lg*) from the UNE, however, are observed to vary with the great circle direction (Figure 2a). Stations (BRD and MDJ) with great circle paths over the continental crust have strong *Lg* waves, while stations (DGY, UCN, ULJ, WSN, BUS, and KRN) with great circle paths crossing the continental margin have weak *Lg* energy. The stations (SEO, SES, and CHC) with great circle paths that partly cross the structure beneath the Sea of Japan (East Sea) have an intermediate-strength *Lg* phase (Figure 2a). The peak-to-peak amplitudes of *Lg* phases for the UNE are presented in Figure 5a. The extinction of the *Lg* phase along a path that includes a thin crust is well documented [*Ewing et al.*, 1957; *Kennett*, 1986]. These observations have been confirmed with numerical models [*Zhang and Lay*, 1995; *Kennett and Furumura*, 2001].

[10] The *Lg* amplitude variation by raypath is consistently observed in the records for event A, which shows a similar great circle path distribution (Figure 2b). The record sections for which great circle paths are mainly (or fully) over continental crust display prominent *Lg* energy (Figure 3). Regional seismic waves from event B travel great circle paths that lie entirely along the continental crust. Event C observations consist of great circle paths that cross the continental margin. The crustally guided shear waves are clearly observed to distances of 790 km for event B and 420 km for event C, despite relatively low magnitudes (Figures 2c, 2d, and 5c).

3.1. Waveforms From Continental Margin Paths

[11] Comparison of seismic records at similar epicentral distances allows us to examine the waveform variation with raypaths (Figure 4). Since the distances are similar, we assume that the geometrical-spreading effect can be ignored. Stations UCN and DGY are to the east relative to stations SEO and CHC. Stations UCN and DGY have longer continental margin paths than stations SEO and CHC. The records from the stations with primarily continental paths (western stations; SEO and CHC) display strong *Lg* phases, while those with longer continental margin paths (eastern stations; UCN and DGY) display weak *Lg* phases (Figure 4b). This feature is consistently observed in the station pairs for event A as well (Figure 4d). Note that the distribution of great circle paths for event A is similar to that for the UNE. In addition, the magnitudes of the two events are comparable (M4.2 for UNE, M4.1 for event A). We also observe that stations at similar distances display different *Sn* composition for both the UNE and event A; station DGY displays a strong *Sn* phase, while station CHC shows a weak *Sn* phase (Figures 4b and 4d).

[12] We now compare the spectra of *Sn* and *Lg* between two nearby stations, CHC and DGY (Figure 6). The spectra of station BRD, which lies on a pure continental raypath, are presented for reference. Here the epicentral distances (L) from the events (UNE and event A) to station CHC are very close to those to station DGY: L = 406.6 km (CHC) and 402.1 km (DGY) for the UNE and L = 327.9 km (CHC) and

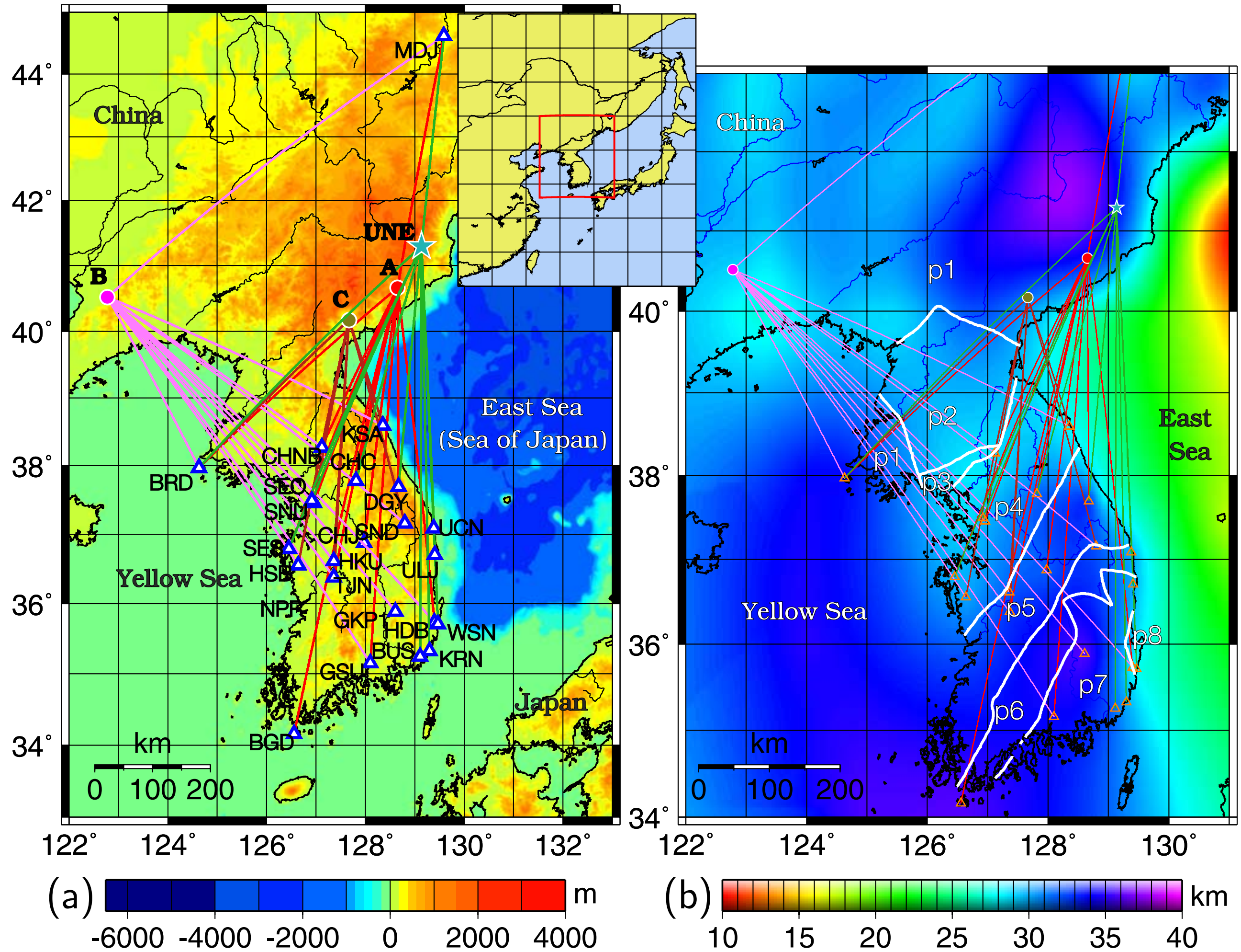

Figure 1. Distribution of events, stations, and major geological structures in the Korean Peninsula. (a) Locations of events and stations on a surface topography map. The nuclear explosion (star) in North Korea and three natural earthquakes (circles) are analyzed. Broadband records are collected from stations in southern Korea and China (triangles). The great circle paths are drawn with solid lines. (b) Major geological structures (p1, Nangrim Massif; p2, Pyongnam Basin; p3, Imjingang Fold Belt; p4, Kyonggi Massif; p5, Okchon Fold Belt; p6, Yongnam Massif; p7, Kyongsang Basin; p8, Pohang Basin) and crustal thickness variation in and around the Korean Peninsula (compiled from *Chang and Baag* [2005] and *Yu* [2006]). The average crustal thickness in the Korean Peninsula is ∼32 km. The geological structure is characterized by three massifs and intervening fold belts. The crustal thickness decreases rapidly with distance from the eastern shore toward the Sea of Japan (East Sea).

329.5 km (DGY) for event A. The epicentral distances from the events to station BRD are 534.6 km for the UNE and 457.7 km for event A.

[13] Adaptive time windows, whose durations depend on the distances, are applied for sampling *Sn* and *Lg* phases from the records. The time windows range between 20 and 22 s for both *Sn* and *Lg*. A cosine taper with a length of 0.12 s is applied at the ends of the time window. The calculated spectra are smoothed using a 0.4-Hz moving window. For azimuth-independent comparison, we calculate horizontal spectra from a root-mean-square of E-W and N-S spectra. The vertical spectra are obtained from vertical seismograms.

[14] The dominant frequency contents of both *Sn* and *Lg* are between 0.5 and 2 Hz (Figure 6), which agrees with previous regional observations [e.g., *Hong and Xie*, 2005]. The *Sn* spectra for station DGY are stronger than those for station CHC in the frequency range of 1–8 Hz (m4 in Figure 6). On the other hand, the *Lg* spectra for station CHC are stronger than those for station DGY in the same band (see m2 and m3 in Figure 6). Thus it is shown that *Lg* develops along the continental path while *Sn* is strong along the continental margin path. The negative correlation be-

Table 1. Source Parameters of the Events Analyzed in This Study

Event	Date	Latitude, °N	Longitude, °E	Depth, km	Magnitude
UNE[a]	09/10/2006	41.29	129.13	0	m_b4.2
Event A	16/04/2002	40.66	128.65	10	m_b4.1
Event B	18/06/2006	40.52	122.78	0	M_L3.6
Event C	30/06/2006	40.12	127.67	1	M_L3.0

[a]U.S. Geological Survey estimates.

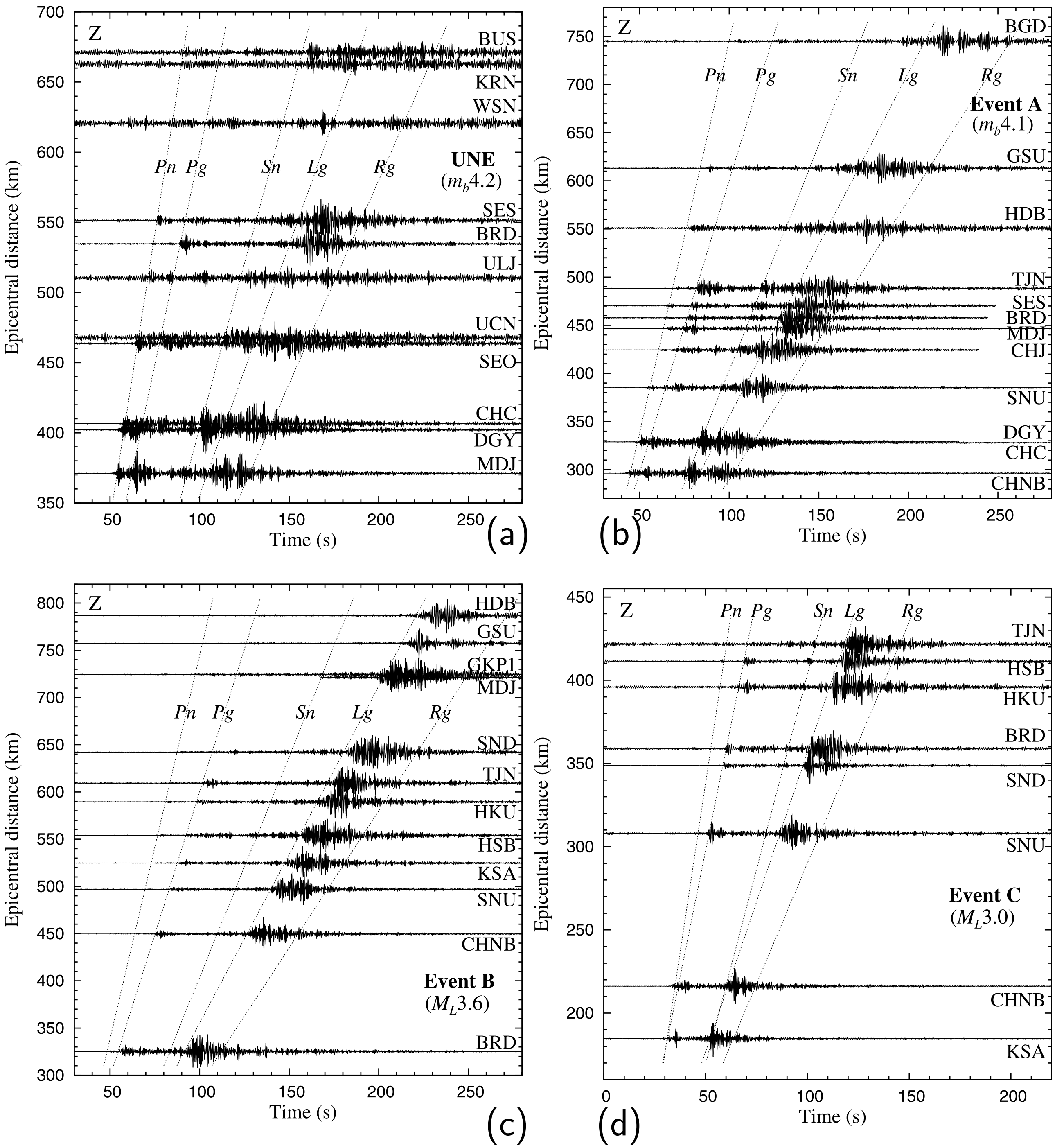

Figure 2. Vertical velocity seismograms of (a) the underground nuclear explosion (UNE) and three natural earthquakes ((b) event A, (c) event B, (d) event C) in Figure 1, which are band-pass filtered between 0.8 and 2.2 Hz. The primary regional phase arrival times from a crustal model [*Chang and Baag*, 2005] are marked with dotted lines. The amplitudes of regional phases from the UNE and event A appear to vary with station; some stations at nearer distances display weaker signals than those at longer distances (e.g., ULJ and BRD, respectively, in Figure 2a; HDB and GSU, respectively, in Figure 2b). Stations on raypaths crossing the continental margin display weak signals. Regional seismograms from event B, which travel along pure continental raypaths to stations, display strong regional phases despite their low magnitude (see Table 1). Each trace is normalized by its maximum amplitude.

tween *Lg* and *Sn* energy suggests that there is an energy transfer between *Sn* and *Lg*. Here it appears that the energy conversion between *Sn* and *Lg* depends on the crustal properties along the raypath. This raypath-dependent feature is consistently observed in records for both the UNE and event A. Since the epicentral locations and the source types are different between the UNE and event A, we can confirm that the observed feature is not caused by inherent source

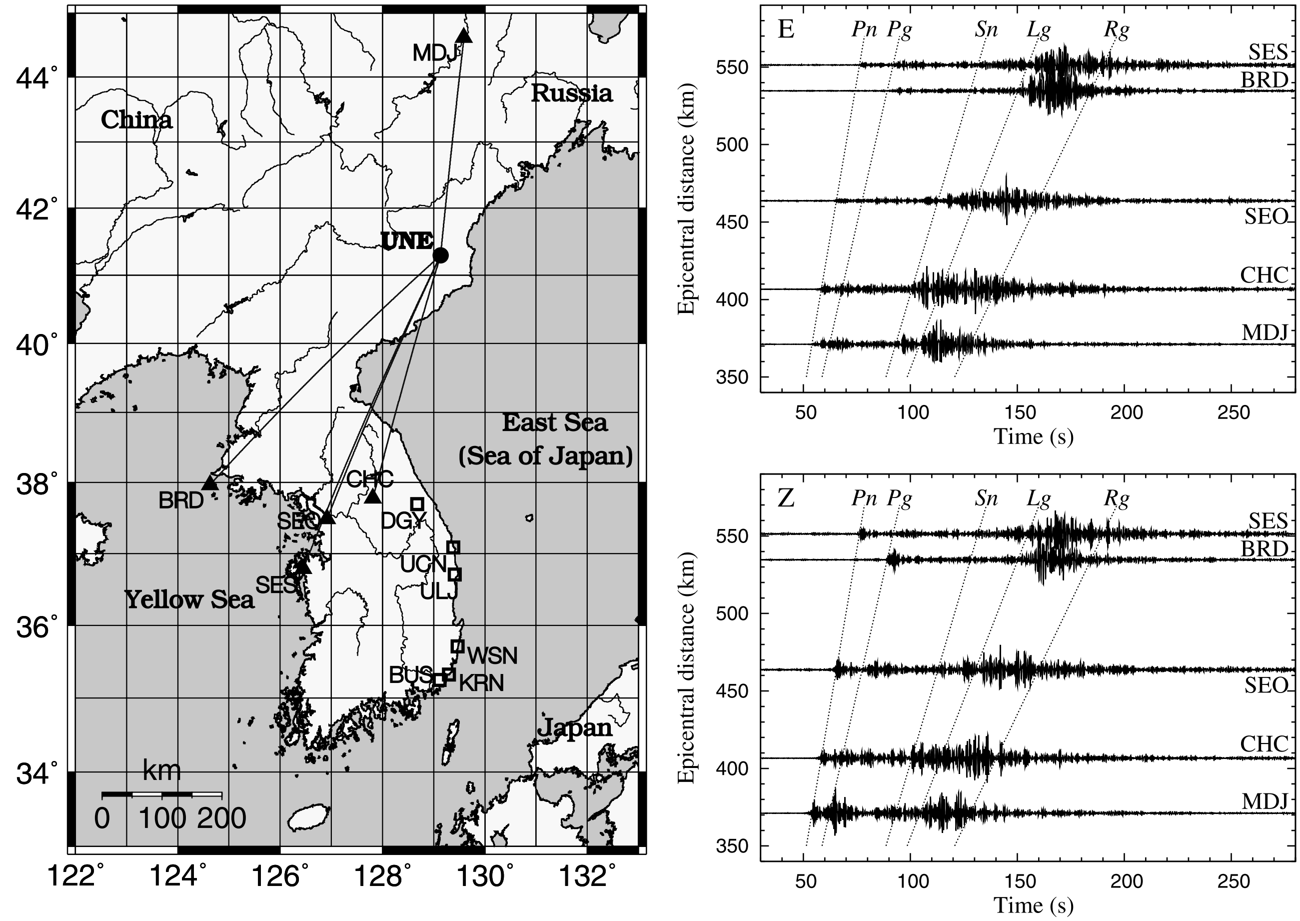

Figure 3. Distribution of stations (solid triangles) recording strong *Lg* phase arrivals from the UNE (solid circle). The seismograms in E-W (E) and vertical (Z) components are presented in the right column. Stations recording weak *Lg* phases are marked with open squares (see also Figure 2a). The great circle paths to the stations with strong *Lg* arrivals are marked with solid lines on the map. The stations with strong *Lg* phases are on continental paths, while those with weak *Lg* phases are on continental margin paths. Each trace was normalized by its maximum amplitude.

properties. Thus it appears that the difference in waveforms may be caused by the difference in raypath properties.

[15] The locations of stations DGY and MDJ relative to the UNE constitute a geometry in which the stations lie at similar distances but in opposite azimuthal directions (DGY: 185.8°, 402.1 km; MDJ: 5.6°, 371.1 km) (Figure 4). Station MDJ lies along a pure continental path, and station DGY lies along a continental margin path. The radiated energy from a vertically symmetric source is azimuthally isotropic, which is expected during a nuclear explosion, with cone-shaped rock cracking [*Massé*, 1981] and spalling [*Day and McLaughlin*, 1991]. Assuming an isotropic source, the radiated energies from the UNE to stations DGY and MDJ are nearly equivalent to each other. This assumption allows us to compare the crustally guided waves (*Pg* and *Lg*) between stations DGY and MDJ. We find that the crustally guided energy is weak in the station on the continental margin path (DGY), while strong in the station on the pure continental path (MDJ) (Figure 4).

[16] Raypath-dependent waveform variation appears to be particularly strong at 1 Hz (Figure 5). This may be because 1-Hz shear waves are well trapped in the crust and are highly influenced by crustal structures. The lateral variation of crustal structures (e.g., Moho undulation) causes dissipation of *Lg* because of energy leakage into the mantle [e.g., *Kennett*, 1986]. Thus the low *Lg* amplitudes at stations with continental margin paths appear to be associated with the raypath effect.

3.2. Waveforms From Pure Continental Paths

[17] We examine the spectral content of *Lg* for stations on continental paths and test the inference that high-frequency energy is attenuated by the interference of rifted crust along the continental margin. Event B occurred near the western border between China and North Korea. Thus the great circle paths from event B to stations in southern Korea and China pass over the continental crust (Figure 1), including the crust beneath the Yellow Sea, which is known to be a continental crust.

[18] We divide the data set for event B into three distance ranges, L = 320–450 km, 500–640 km, and 720–790 km. The spectral variations with distance are presented in Figure 7. The spectral amplitudes of both horizontal and vertical components decrease with distance in the frequency range of 1–8 Hz, regardless of azimuths. We infer that the characteristic amplitude variations observed in records from

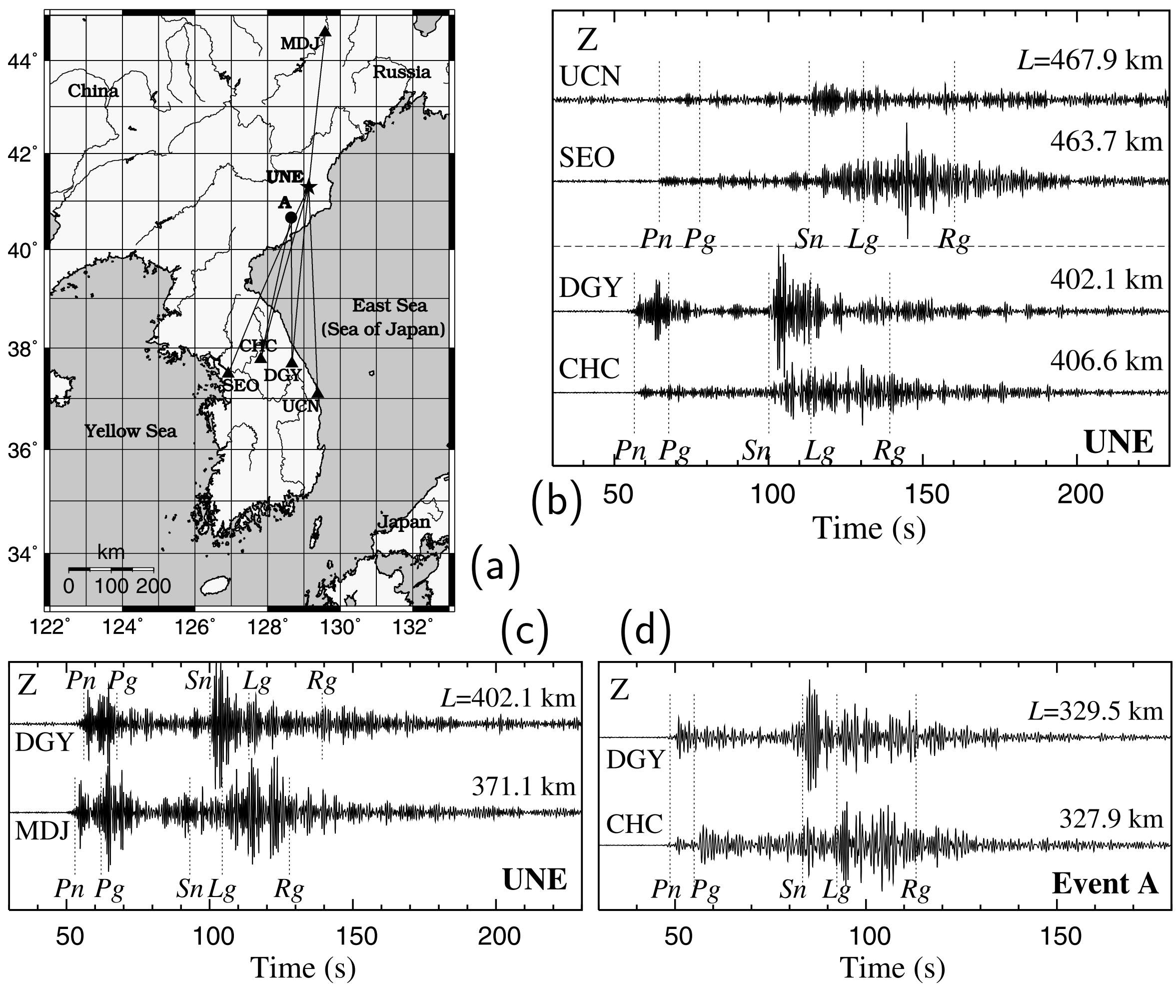

Figure 4. Comparisons of seismograms for selective pairs of stations. (a) Map of stations and events used. (b) Comparisons of vertical component records between stations with similar epicentral distances (UCN–SEO and DGY–CHC). (c) Comparison of UNE records at two stations with azimuths that vary by nearly 180°. (d) Comparison of event A seismograms at stations with similar epicentral distances (DGY–CHC). In each pair of records, the top record is for a station on an uplifted crust path, and the bottom one is for a station on a marginal uplifted crust path or a pure continental path. Event A observations are along similar great circle paths to the UNE. Similar waveform variations are observed for both the UNE records and the event A records. The epicentral distances (L) are annotated. Every record is normalized by the maximum amplitude in the *Pn* window.

stations with continental margin paths are associated with the crustal structure.

[19] The strong *Lg* development at stations on continental paths at frequencies around 1 Hz (see records at BRD and MDJ for the UNE and event A; records at all stations for event B) may be associated with wavelength (frequency)-dependent energy trapping in the crust [*Kennett*, 1986]. That is, seismic waves at frequencies around 1 Hz are favorably trapped in the continental crust, which has an average crustal thickness of ~32 km [*Chang and Baag*, 2005]. However, low-frequency crustal-guided energy leaks across the Moho in the thin crust of the continental margin (CHC and DGY in Figure 6). We do not find, however, such strong 1-Hz energy in the mantle lid shear wave phase (*Sn*) recorded at stations on continental paths (Figures 6a and 6b). This observation suggests that the 1-Hz energy is associated with energy trapping in the crust.

[20] We, however, observe enhanced *Sn* phases in records from stations on continental margin paths. The *Lg* phase is weak at these stations. This suggests that the *Sn* enhancement and *Lg* weakening along continental margin paths (Figures 4c and 4d) result from *Lg* energy leaking from the uplifted crust into the mantle, causing successive development of mantle lid waves.

4. Comparison With Numerical Simulation

[21] We conduct a numerical simulation of seismic wave propagation to investigate the variations in waveform and spectral content for changes in crustal structures along the waveguide. We consider four crustal models that include a horizontally layered model, a crustal pinch model, a magma-underplating model, and a bulgy layer model (Figure 8).

[22] The crustal pinch model roughly reflects the crustal structure in the region between the UNE and station DGY.

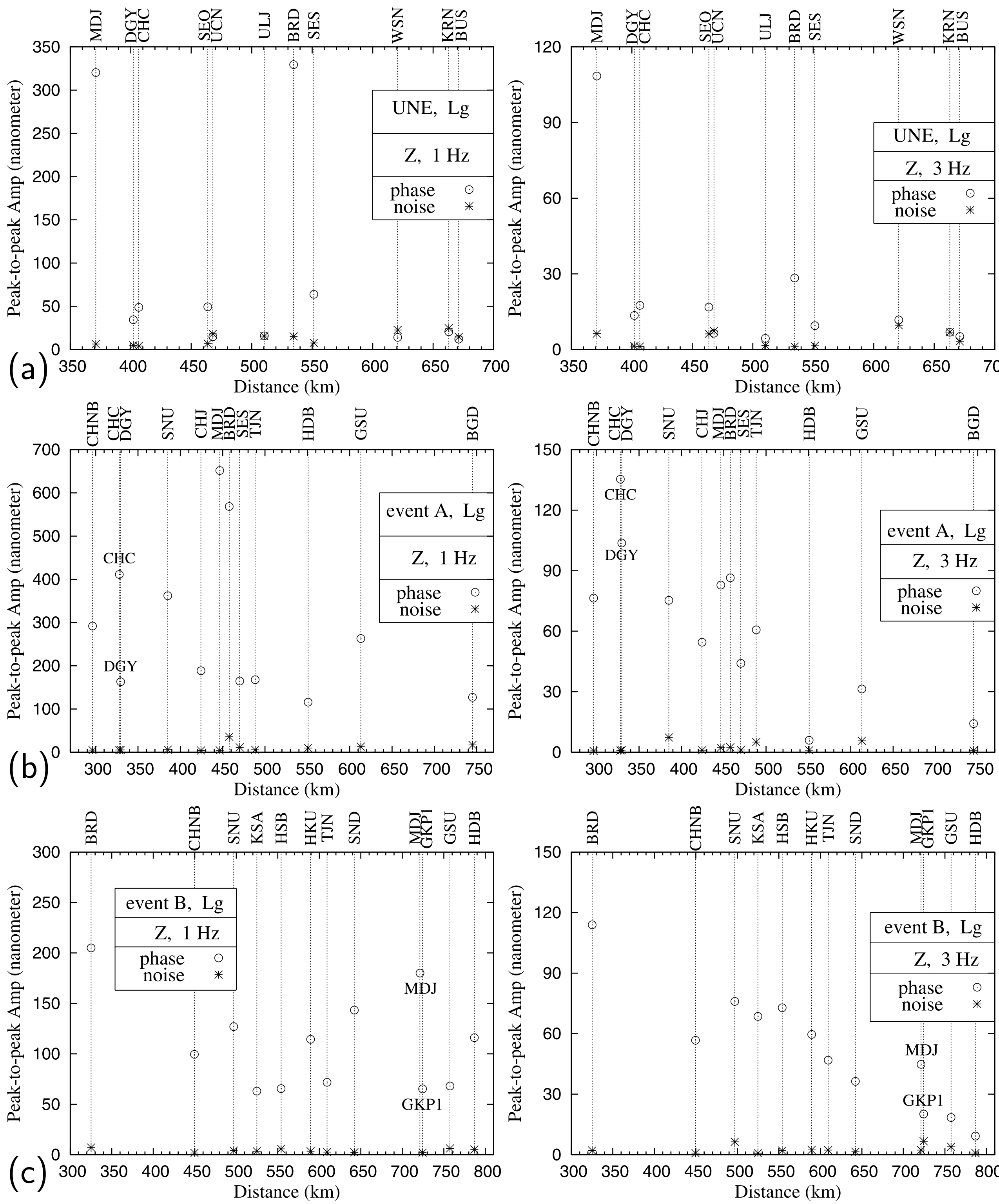

Figure 5. Peak-to-peak *Lg* amplitudes from seismic records for (a) the UNE, (b) event A, and (c) event B. The amplitudes for band-passed waveforms at 1 Hz are presented in the left column, and those for 3 Hz are presented in the right column. The 1-Hz amplitudes vary with the crustal structure along the raypath, while the 3-Hz amplitude generally decreases with distance. The amplitudes of background noises are also presented. High *Lg* amplitudes are observed in records from stations on continental paths (stations MDJ and BRD) for the UNE and event A. The 1-Hz *Lg* amplitude for event B does not vary much by station, and the 3-Hz amplitude displays the effect of geometrical spreading.

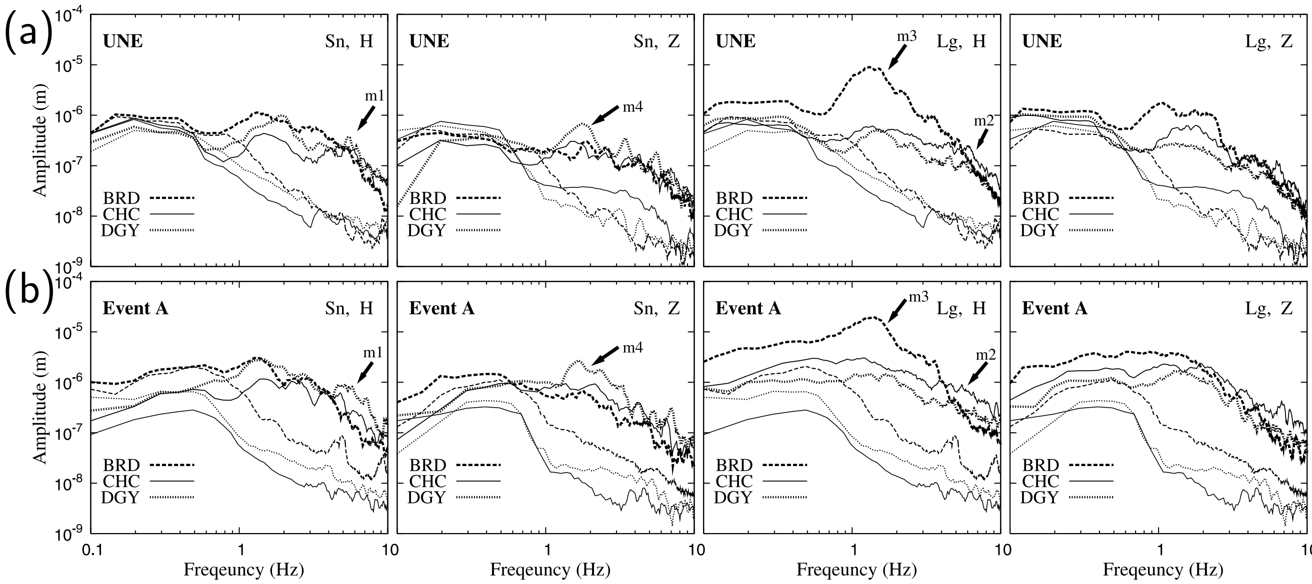

Figure 6. Velocity spectra (bold lines) of *Sn* and *Lg* phases at stations BRD, CHC, and DGY for the UNE and event A. The velocity spectra of background noise are presented with thin lines. Adaptive time windows with durations between 20 and 22 s, depending on the distances, are applied. The description for the time window is given in the text. (a) Velocity spectra of *Sn* and *Lg* from the UNE and (b) those from event A. Both horizontal and vertical spectra are presented. Station BRD is on a pure continental path, station DGY is on a path with a major continental margin component, and station CHC is on a path with a minor continental margin component. The signals from the UNE are greater than the noise at frequencies higher than 0.5 Hz. The station on the continental path (BRD) has significant *Lg* energy at around 1–2 Hz (m3), while the station on the uplifted crust path (DGY) shows a strong *Sn* phase around the same frequency range (m4). Characteristic phase enhancement depending on the raypath is observed in records for stations DGY and CHC. Station DGY has stronger *Sn* than station CHC at frequencies in the range of 1–8 Hz (m1), and station CHC has stronger *Lg* than station DGY in the same frequency range (m2).

We set the height of the crustal pinch on the Moho to be 8.2 km, considering the crustal thickness model in Figure 1b. We modulate the height of uplifting in each layer to decrease gradually with distance from the Moho. The magma-underplating model represents a crustal structure with intrusive magma at the boundary between the mantle and crust. This magma underplating is believed to be present in the region beneath the eastern shore of the southern Korean Peninsula [*Cho et al.*, 2004]. The last model, the bulgy layer model, is a common crustal structure that is associated with tectonic deformation.

[23] A 1-D crustal velocity model of *Chang and Baag* [2006] is employed for the properties of each layer. The *P* and *S* wave velocities (α_j, β_j, j = 1, 2, 3, and 4) are α_j = 5.67, 6.05, 6.67, and 7.88 km s^{-1} and β_j = 3.27, 3.49, 3.85, and 4.55 km s^{-1}, respectively. Also, the densities (ρ_j) are ρ_j = 2.58, 2.71, 2.90, and 3.29 g cm^{-3}. We set the properties of the underplating layer in the underplating model to be the mean properties between the third and fourth layers, i.e., α_i = 7.28 km s^{-1}, β_i = 4.2 km s^{-1}, and ρ_i = 3.1 g cm^{-3}. The thicknesses of the layers in the horizontally layered medium are h_1 = 5.1 km, h_2 = 11.6 km, and h_3 = 15.2 km. The Moho in the horizontally layered medium is located at a depth of 31.9 km. The thicknesses of the uplifted regions in the crustal pinch model are h_1 = 3.7 km, h_2 = 8.45 km, and h_3 = 11.05 km. The Moho beneath the uplifted layers is located at a depth of 23.2 km. The thickness of the intrusive magma in magma-underplating model is 7.55 km. The thickness of the bulgy layer of the last model is 15.45 km.

[24] In order to understand the waveform variation of shear waves (*Sn* and *Lg*) according to crustal structures, we implement a source that excites both *P* and *S* waves, compromising the influence of the primary nuclear explosion and accompanying secondary sources. Since the dominant energy is excited in the vertical direction by the vertical point force, we analyze the synthetic seismograms on vertical components in this study. In this numerical modeling of seismic wave propagation, the inelastic attenuation effect, which is associated with the inherent medium property, is not considered. This allows us to investigate the sole influence of the lateral variation of crustal structures on the development of regional phases.

[25] We conduct numerical simulation of seismic wave propagation for source time functions. We use Ricker wavelets of seven different frequencies, 0.5, 1, 1.5, 2, 3, 4, and 5 Hz, for the source time functions. A 2-D finite difference method (FDM) based on parallel computation [*Sheen et al.*, 2006] is employed for the simulation. The algorithm is based on the velocity stress staggered grid formulation of the elastic wave equation. The method is fourth-order accurate in space and second-order accurate in time. The size of the model is 750 km by 40 km. The grid spacing is 50 m, and the time step is 2.5 ms. Each model is composed of 15,000 by 800 grid points.

[26] The top boundary of the medium is considered the free surface, and the other artificial boundaries are treated as absorbing boundaries [e.g., *Hong and Kennett*, 2002]. The absorbing boundary conditions are adopted in the FDM

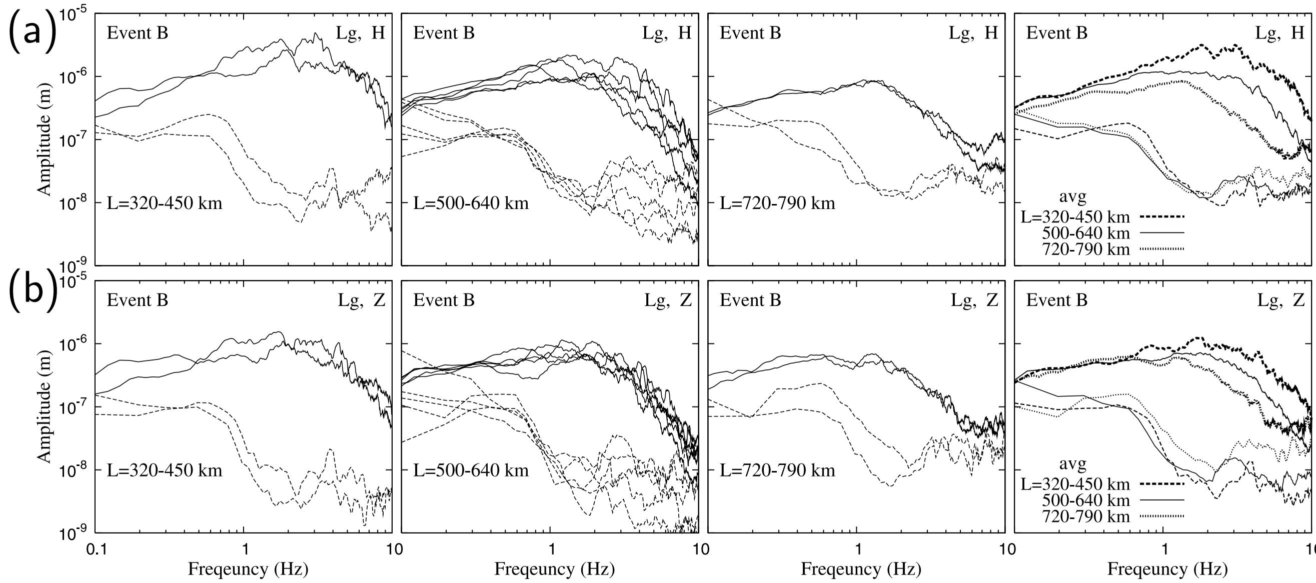

Figure 7. *Lg* velocity spectra (bold lines) of event B for pure continental paths to stations in southern Korea: (a) H and (b) Z components. The spectra of background noise are presented as thin lines. The *Lg* spectra at three distance regimes are presented (L = 320–450 km, 500–640 km, and 720–790 km). The signals are greater than the noise in the whole frequency range. The last column on the right is the average spectrum from each distance regime. Energy between 1 and 8 Hz gradually decreases with distance. Energy at lower frequencies (<1 Hz) shows no apparent variation with distance. This attenuation feature suggests that the *Lg* at CHC and DGY from the UNE and event A was attenuated during propagation along the continental margin paths.

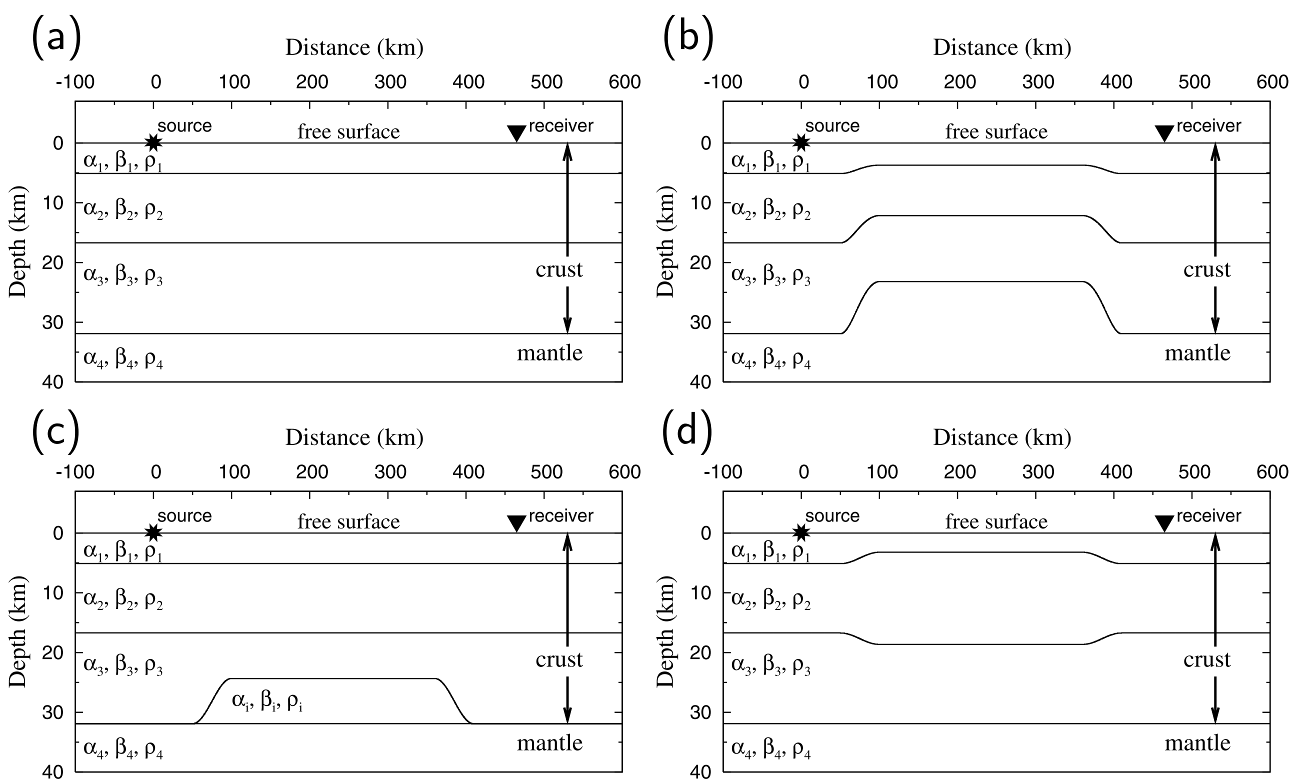

Figure 8. Crustal models for computation of synthetic seismograms: (a) horizontally layered model, (b) crustal pinch model, (c) magma-underplating model, and (d) bulgy layer model. Parameters α_j, β_j, and ρ_j (j = 1, 2, 3, and 4) are the P and S wave velocities and the density at layer j. Parameters α_i, β_i, and ρ_i in the magma-underplating model are the properties of the underplating layer. The source is located at L = 0 km (star), and the receiver is placed at a distance of 465 km (inverted triangle).

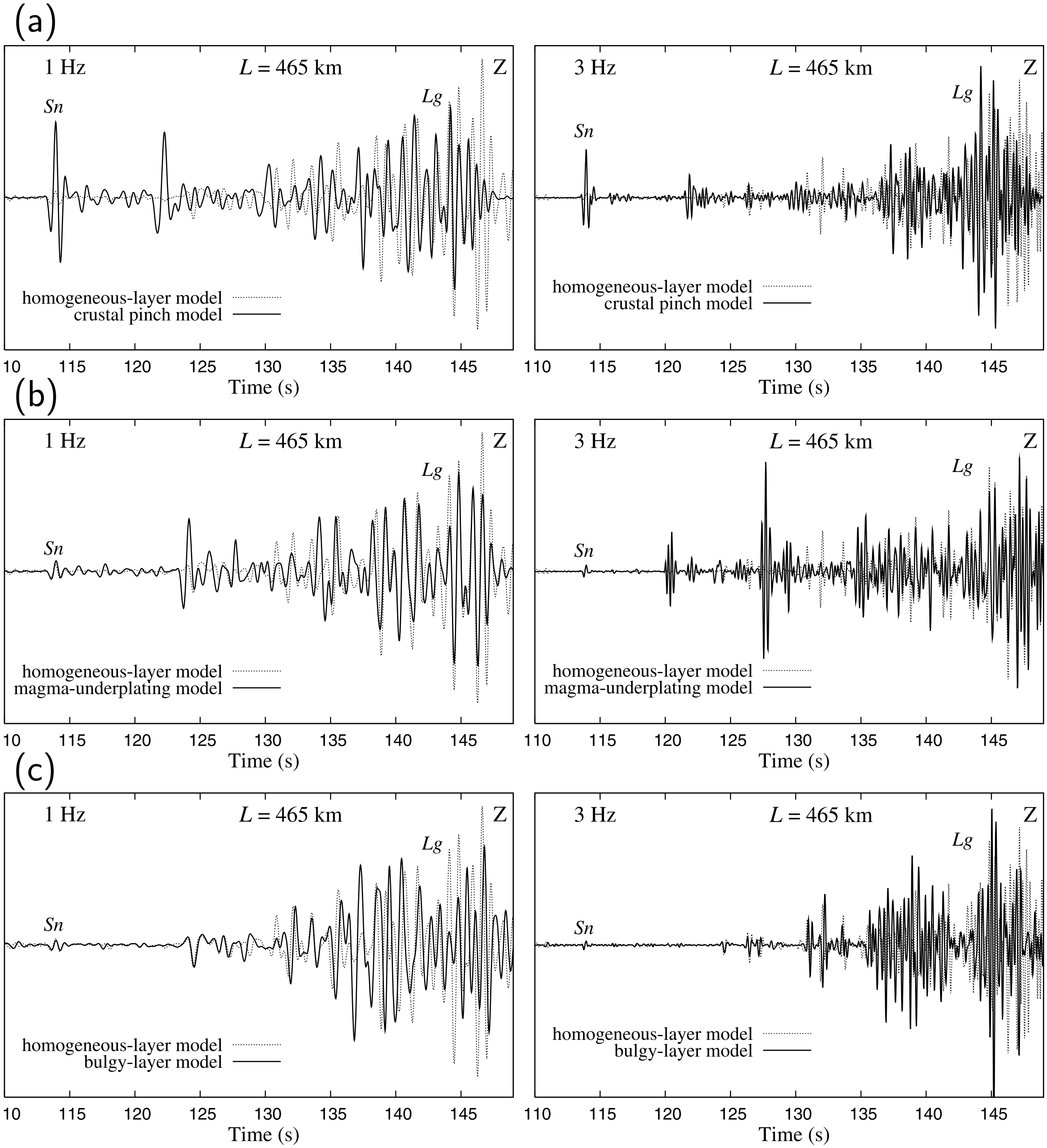

Figure 9. Synthetic seismograms with source time functions of 1 and 3 Hz for the models in Figure 8: (a) crustal pinch model, (b) magma-underplating model, and (c) bulgy layer model. The seismograms for the horizontally layered model are presented for comparison. *Lg* attenuation is observed at 1 Hz for all models, while it is relatively weak at 3 Hz. A strong *Sn* phase develops in the crustal pinch model at both 1 and 3 Hz. The other models do not generate any noticeable variation in the *Sn* phase for both 1 and 3 Hz.

using the perfectly matched layer scheme [*Berenger*, 1994; *Sheen et al.*, 2006]. A vertical point source is applied at the location of L = 0 km in the model, and a receiver is located at a distance of 465 km, a representative distance between the UNE and stations in southern Korea.

[27] A computation of synthetic seismograms to 1 Hz with a time length of 200 s takes 4.74 h on an message passing interface–based IBM cluster with eight nodes, consisting of Power PC970 with dual 2.2-GHz processors and 2 GB of memory. The computation is made for every model at the seven different frequencies. The synthetic seismograms from the 2-D numerical simulations can be readily converted to seismograms in 3-D space by correcting the geometrical spreading effect, which can be achieved

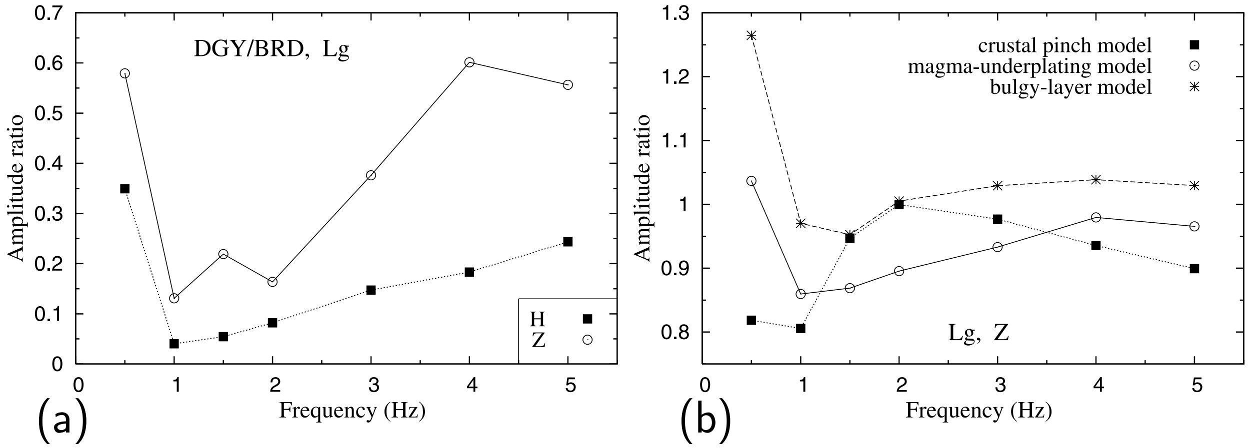

Figure 10. *Lg* amplitude ratios as a function of frequency. (a) *Lg* amplitude ratios between stations DGY and BRD estimated from the spectra in Figure 6 and (b) *Lg* amplitude ratios estimated from synthetic seismic data. Both the magma-underplating model and bulgy layer model present similar forms of amplitude ratio variation to those from field data in Figure 10a. The crustal pinch model exhibits an increase of attenuation at high frequencies ($f > 2$ Hz).

by convolving seismograms with $1/\sqrt{t}$ and differentiating them in time [*Vidale et al.*, 1985; *Hong and Kennett*, 2003]. This technique enables us to economically compute high-frequency 3-D synthetic seismograms for horizontally homogeneous media.

[28] Synthetic seismograms for 1 and 3 Hz, out of those for all seven different frequencies (0.5, 1, 1.5, 2, 3, 4, and 5 Hz), are presented in Figure 9. We compare the synthetic seismograms from the homogeneously layered crustal model with those from the inhomogeneous layer models. We find significant *Lg* attenuation in every inhomogeneous layer model at 1 Hz. The *Lg* attenuation is relatively weak in the inhomogeneous layer models at 3 Hz. A feature observed in the crustal pinch model is the strong development of the *Sn* phase at both 1 and 3 Hz. The other inhomogeneous layer models, however, exhibit little variation in the *Sn* phase. The strong *Sn* development in the crustal pinch model agrees with the field observation in section 3 (Figure 4).

[29] We now quantify the *Lg* amplitude changes from the synthetic seismograms and compare them with field observations (Figure 10). However, the *Lg* amplitude ratios from synthetic seismograms cannot be compared with those from field observations because the simplified crustal models in this study do not incorporate the 3-D lateral variation effect of crustal structures properly. In reality, the crustal thickness in the Sea of Japan (East Sea) gradually decreases with distance from the shoreline, and the tectonic structures around the Korean Peninsula are complex. Also, the inelastic attenuation effect, which may vary with location, is not considered in the numerical modeling. Thus the form of amplitude ratio variation is more informative than the value of the amplitude ratio when inferring the possible causes of *Lg* attenuation.

[30] In Figure 10a, we estimate the *Lg* amplitude ratio between stations DGY and BRD. Here, the geometrical spreading was corrected before calculation of the amplitude ratio. The general features of *Lg* amplitude variation are similar between horizontal and vertical components when the amplitude ratios are smallest at 1 Hz and generally increase with frequency.

[31] The *Lg* amplitude ratios from synthetic seismograms vary according to crustal model (Figure 10b). The *Lg* amplitude ratios from the magma-underplating model and bulgy layer model display similar forms of variation to those from field data. The *Lg* amplitude ratios from the crustal pinch model are smallest at 1 Hz and increase with frequency up to 2 Hz and decrease after 2 Hz. Thus the amplitude ratios from the crustal pinch model appear to agree less with the field observations at high frequency. The strong *Sn* excitation on a continental margin path cannot be explained with either the magma-underplating model or the bulgy layer model but only with the crustal pinch model. This synthetic comparison suggests that the observed waveform variation of seismic records from the continental margin path may be a result of the combined influence of crustal thinning, magma underplating, and/or localized layer bulging.

5. Magnitude Variation

[32] We estimate the magnitude of the UNE from the observed regional records. We examine the magnitude variation with great circle path. Seismic phases *Pn* and *Lg* have different raypaths. Thus they are influenced differently by a change in crustal structure along the great circle direction. We examine the body wave magnitudes for a quantitative study of raypath-dependent phase variation.

[33] The body wave magnitude scale has not been established for the Korean Peninsula yet. We adopt Nuttli's $m_b(Lg)$ scale [*Nuttli*, 1973; *Herrmann and Nuttli*, 1982],

$$m_b(Lg) = -3.10 + 1.66\log(\Delta) + \log(A/T), \qquad (1)$$

where Δ is the epicentral distance in kilometers, A is the peak-to-peak *Lg* amplitude in millimicrons (nanometers), and T is the period. This magnitude scale is valid for the central and eastern United States [e.g., *Nuttli*, 1973; *Kim*,

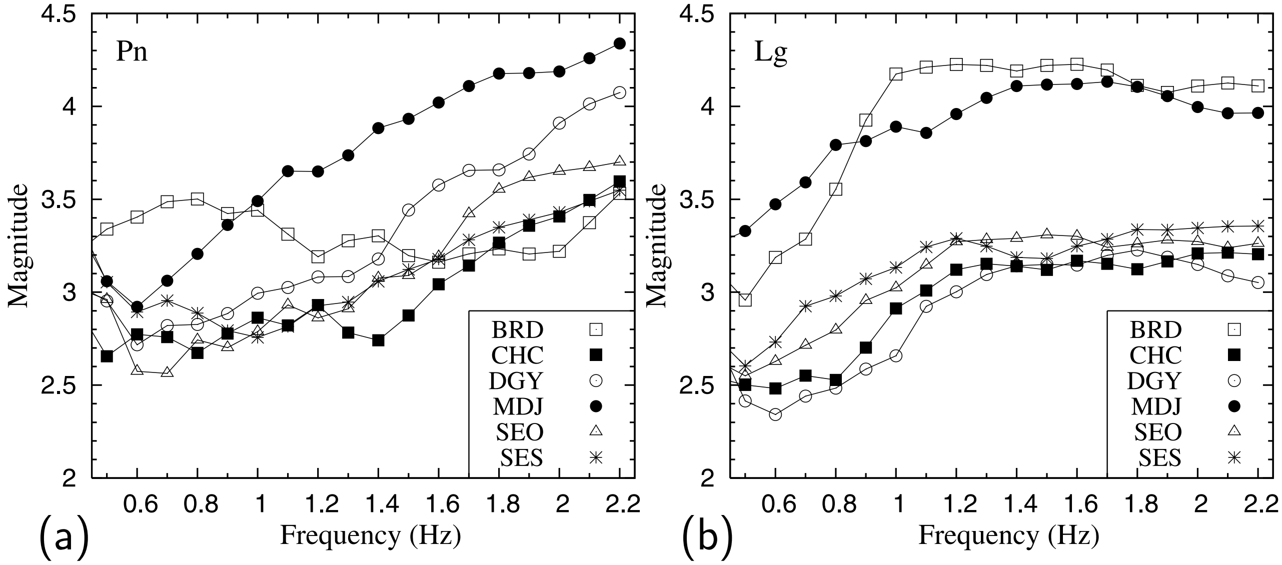

Figure 11. Body wave magnitudes of the UNE as a function of frequency: (a) $m_b(Pn)$ and (b) $m_b(Lg)$. The estimated *Pn* body wave magnitude, $m_b(Pn)$, appears to increase with frequency in general, while the *Lg* body wave magnitude, $m_b(Lg)$, is nearly constant at frequencies over 1 Hz. The estimates of $m_b(Pn)$ range between 2.7 and 4.2 at frequencies in the range of 1.0–2.0 Hz. The estimates of $m_b(Lg)$ significantly vary with the raypaths; $m_b(Lg)$ for records from continental paths (MDJ and BRD) is 3.8–4.2 and that for records from uplifted crust paths (CHC, DGY, SEO, and SES) is 2.4–3.1.

1998]. The Korean Peninsula and the eastern United States are similar in having moderate seismicity and weak crustal attenuation because of hard rock basements [*Jo*, 2007]. This similarity allows us to employ Nuttli's $m_b(Lg)$ scale [*Nuttli*, 1973; *Herrmann and Nuttli*, 1982] for estimating the magnitudes of regional events in the Korean Peninsula.

[34] Similarly, we apply the $m_b(Pn)$ scale for the eastern United States as given by *Evernden* [1967],

$$m_b(Pn) = -3.27 + 2\log(\Delta) + \log(A/T), \qquad (2)$$

where A is the zero-to-peak *Pn* amplitude in nanometers and other parameters are the same as those in equation (1). This *Pn* body wave magnitude scale is valid also for the Chinese territory [*Zhou et al.*, 2006]. We measure both *Pn* and *Lg* body wave magnitudes from equations (1) and (2).

[35] We estimate the magnitudes as a function of frequency from 0.5 to 2.2 Hz at every 0.1 Hz, which are the dominant frequencies of the regional phases (Figure 6) [*Hong and Xie*, 2005]. The magnitude is determined from displacement seismograms that are deconvolved with the instrument responses and band-pass filtered around the frequency of interest.

[36] The estimates of $m_b(Lg)$ and $m_b(Pn)$ of the UNE are presented in Figure 11. It appears that $m_b(Pn)$ increases with frequency, while $m_b(Lg)$ is stable at frequencies over 1 Hz. The estimated $m_b(Pn)$ is shown to be less dependent on the raypath but is distributed in a wide magnitude range of 2.7–4.2 in the frequencies between 1.0 and 2.0 Hz. When we exclude stations MDJ and DGY that are either at the shortest distance or on the uplifted crustal path, the magnitudes range between 2.7 and 3.7. Here the magnitude $m_b(Lg)$ appears to be classified by the type of raypath; the $m_b(Lg)$ from records on continental paths (BRD and MDJ) ranges from 3.8 to 4.2 in the frequencies between 1.0 and 2.0 Hz, while those from records on continental margin paths (CHC, DGY, SEO, and SES) are distributed in a range of 2.6–3.4 on the same frequency band.

[37] We additionally compare the $m_b(Lg)$ of events A and B to examine if the magnitude varies with raypath properties. Note that the raypaths of event A are continental margin paths that are very similar to those of the UNE. In contrast, the raypaths of event B are pure continental paths (see Figure 1). The characteristic $m_b(Lg)$ difference between pure continental and continental margin paths is distinctive among the magnitude estimates in event A, which is consistent with the observation in the UNE (Figure 12a). On the other hand, the $m_b(Lg)$ of event B is distributed in a narrow range of magnitude in the frequencies between 1.0 and 2.0 Hz (Figure 12b). These observations confirm that the crustal-guided waves are significantly dissipated during propagation through the undulated continental margin.

6. *Lg Q* Variation

[38] To quantify the *Lg* attenuation with raypaths, we measure the *Lg* attenuation factor (Q) using a coda normalization method that determines the *Lg* attenuation by comparing the amplitudes between *Lg* and coda [e.g., *Sato and Fehler*, 1998; *Chung and Lee*, 2003]. This coda normalization technique is useful when the radiated energy from the source is unknown, which is the case for most field observations.

[39] The *Lg* amplitude (A_{Lg}) can be expressed by [e.g., *Fan and Lay*, 2002; *Chung and Lee*, 2003]

$$A_{Lg}(L,f) = R_{\theta,\phi}S(f)I(f)G(f)L^{-\gamma}\exp[-L\pi/(QU)], \qquad (3)$$

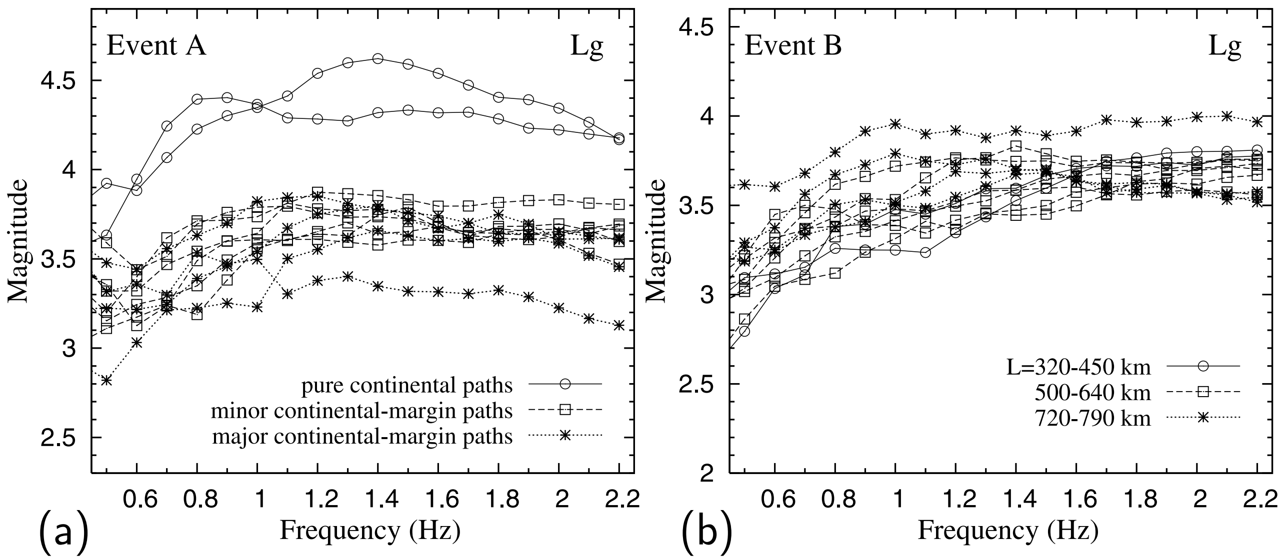

Figure 12. Magnitude estimates at various frequencies from 0.5 to 2.2 Hz: $m_b(Lg)$ of (a) event A and (b) event B. The raypath distribution for event A is similar to that for the UNE. Event B constitutes pure continental paths to the stations in southern Korea. The estimates of $m_b(Lg)$ for event A are classified into three groups by the raypath type in Figure 12a, including the pure continental path group (BRD and MDJ), the minor continental margin path group (CHNB, BGD, CHC, SES, SNU, and TJN), and the major continental margin path group (CHJ, DGY, GSU, and HDB). The pure continental path group displays higher magnitudes than the continental margin path groups, which is consistent with the observation from the UNE in Figure 11. The magnitude estimates for event B yield stable measurements among stations, without any apparent variation with distance.

where L is the distance, f is the frequency, $R_{\theta,\phi}$ is the radiation pattern of the source, $S(f)$ is the source excitation, $I(f)$ is the instrument response, $G(f)$ is the receiver site amplification, γ is the geometrical-spreading factor, and U is the group velocity of Lg. The radiation pattern of Lg, $R_{\theta,\phi}$ can be assumed to be independent from azimuth because of multiple interferences between crustal reflection phases [*Shih et al.*, 1994; *Fan and Lay*, 2002]. We set the geometrical spreading factor to be 0.5 and the group velocity of Lg to be 3.5 km s^{-1} [*Fan and Lay*, 2002].

[40] In a similar way, the amplitude of regional coda can be written by [*Yoshimoto et al.*, 1993]

$$A_{\mathrm{coda}}(f, t_c) = S(f)I(f)G(f)P(f)|_{t=t_c}, \tag{4}$$

where t_c is the time in which the coda amplitude is measured and $P(f)$ is a constant for coda excitation strength. Here the time t_c is a function of distance and Lg group velocity. We choose the time t_c to be 1.5 times the Lg traveltime considering the level of background noise and the

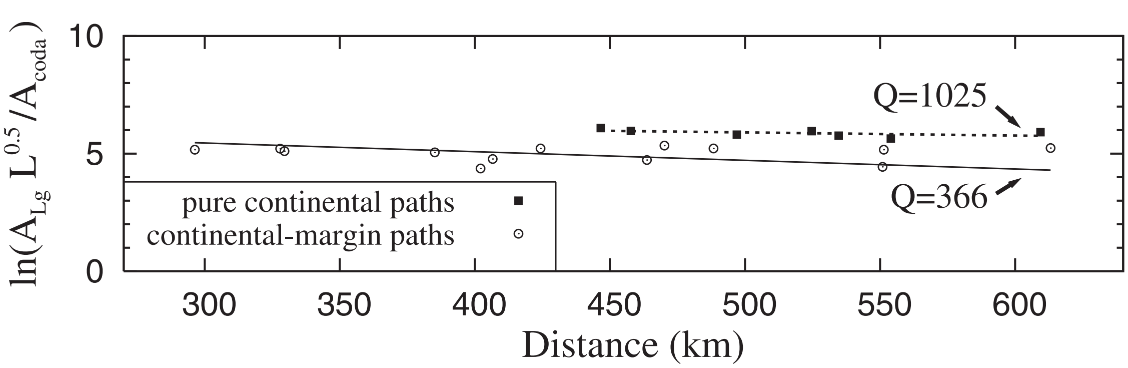

Figure 13. *Lg Q* variation by raypaths. The data are logarithms of amplitude ratios between *Lg* and coda, with geometrical spreading correction. The data from pure continental paths are marked with solid squares, and those from the representative *Lg Q* values are determined using linear regression (solid and dotted lines). The *Lg Q* is determined as 1025 for the pure continental paths and 366 for the continental margin paths.

separation from *Rg*. From equations (3) and (4), a logarithmic expression of $A_{Lg}L^{\gamma}/A_{\mathrm{coda}}$, is given by [e.g., *Chung and Lee*, 2003]

$$\ln\left[\frac{A_{Lg}(L,f)L^{\gamma}}{A_{\mathrm{coda}}(f,t_c)}\right] = -\frac{\pi f}{QU}L + c(f), \quad (5)$$

where $c(f)$ is a constant for the logarithmic ratio between $R_{\theta,\phi}$ and $P(f)$.

[41] From equation (5), we measure the *Lg* quality factor at 1.5 Hz, which is the most dominant frequency of *Lg*. The data are separated into two groups: the pure continental path group and the continental margin path group (Figure 13). The pure continental path group is composed of records of stations MDJ and BRD for the UNE and event A and those of all stations for event B. The continental margin path group is composed of records of the other stations for the UNE and event A. We fit the data sets with lines using a linear regression.

[42] The *Lg* quality factors are estimated as 1025 for pure continental paths and 366 for continental margin paths. Thus *Lg* from continental margin paths is severely attenuated during propagation compared with that from pure continental paths. It is noteworthy that the *Lg Q* from the pure continental paths is higher than the reported average *Lg Q* value in southern Korea at 1.5 Hz, namely, 714 [*Chung et al.*, 2005]. On the other hand, the *Lg Q* from the continental margin paths is lower than the average *Lg Q* in southern Korea. The average *Lg Q* between pure continental and continental margin paths is close to the reported *Lg Q*. This indicates that the *Lg* observed in southern Korea should be corrected for this discriminative attenuation for the determination of magnitude.

7. Discussion and Conclusions

[43] The *Lg* wave, a crustal-guided shear wave, is typically the most dominant phase at regional distance for both nuclear explosions and natural earthquakes. Thus the *Lg* wave is an important phase to deduce the size of the source. The recent nuclear explosion test in North Korea allows us to examine the UNE waveform variation with crustal structure. The *Lg* waves from continental margin paths are significantly attenuated, while those from normal continental paths are stably constructed. The dissipation of *Lg* waves along continental margin paths is caused by the continuous energy leakage into the mantle due to the Moho undulation around the continental margin beneath the Sea of Japan (East Sea). The observed waveform and spectral variations from the UNE with changes to the raypath were confirmed by numerical simulations and comparisons with records of natural earthquakes. Fractional *Lg* energy dissipates in the uplifted crust of the continental margin and eventually develops into a mantle lid wave. This discriminative *Lg* energy attenuation at the continental margin causes underestimation of the magnitudes of regional and local events. Thus amplitude correction considering raypaths is necessary for the correct estimation of magnitude. Alternatively, only the records from continental paths could be used for the determination of magnitude.

[44] **Acknowledgments.** We thank the Korea Meteorological Administration (KMA), the Korea Institute of Nuclear Safety (KINS), and the Incorporated Research Institutions for Seismology (IRIS) for making the UNE records available. We acknowledge that the seismic data for natural earthquakes were collected from the Korea Institute of Geoscience and Mineral Resources (KIGAM), KMA, and IRIS. We are grateful to Sang Hoon Yu for the crustal thickness data inferred from a gravity anomaly and Hyun-Moo Cho and Sung-Joon Chang for their discussion of the crustal structures of southern Korea. The paper benefited greatly from the constructive comments by Brian Stump and three anonymous reviewers. This work was supported by the Korea Meteorological Administration Research and Development Program under grant CATER 2007-5111.

References

Berenger, J. P. (1994), A perfectly matched layer for the absorption of electromagnetic waves, *J. Comput. Phys.*, *114*, 185–200.

Chang, S.-J., and C.-E. Baag (2005), Crustal structure in southern Korea from joint analysis of teleseismic receiver functions and surface-wave dispersion, *Bull. Seismol. Soc. Am.*, *95*, 1516–1534.

Cho, H.-M., H.-J. Kim, H.-T. Jou, J.-K. Hong, and C.-E. Baag (2004), Transition from rifted continental to oceanic crust at the southeastern Korean margin in the East Sea (Japan Sea), *Geophys. Res. Lett.*, *31*, L07606, doi:10.1029/2003GL019107.

Cho, H.-M., C.-E. Baag, J. M. Lee, W. M. Moon, H. Jung, K. Y. Kim, and I. Asudeh (2006), Crustal velocity structure across the southern Korean Peninsula from seismic refraction survey, *Geophys. Res. Lett.*, *33*, L06307, doi:10.1029/2005GL025145.

Chough, S. K., S.-T. Kwon, J.-H. Ree, and D. K. Choi (2000), Tectonic and sedimentary evolution of the Korean peninsula: A review and new view, *Earth Sci. Rev.*, *52*, 175–235.

Chung, T.-W., and K. Lee (2003), A study of high-frequency Q_{Lg}^{-1} in the crust of South Korea, *Bull. Seismol. Soc. Am.*, *93*, 1401–1406.

Chung, T.-W., Y. K. Park, I. B. Kang, and K. Lee (2005), Crustal Q_{Lg}^{-1} in South Korea using the source pair/receiver fair method, *Bull. Seismol. Soc. Am.*, *95*, 512–520.

Day, S. M., and K. L. McLaughlin (1991), Seismic source representations for spall, *Bull. Seismol. Soc. Am.*, *81*, 191–201.

Evernden, J. F. (1967), Magnitude determination at regional and near-regional distances in the United States, *Bull. Seismol. Soc. Am.*, *57*, 591–639.

Ewing, M., W. S. Jardetsky, and F. Press (1957), *Elastic Waves in Layered Media*, McGraw-Hill, New York.

Fan, G., and T. Lay (2002), Characteristics of *Lg* attenuation in the Tibetan Plateau, *J. Geophys. Res.*, *107*(B10), 2256, doi:10.1029/2001JB000804.

Fisk, M. D. (2006), Source spectral modeling of regional *P/S* discriminants at nuclear test sites in China and the former Soviet Union, *Bull. Seismol. Soc. Am.*, *96*, 2348–2367.

Herrmann, R. B., and O. W. Nuttli (1982), Magnitude: The relation of M_L to m_{bLg}, *Bull. Seismol. Soc. Am.*, *72*, 389–397.

Hong, T.-K., and B. L. N. Kennett (2002), On a wavelet-based method for the numerical simulation of wave propagation, *J. Comput. Phys.*, *183*, 577–622.

Hong, T.-K., and B. L. N. Kennett (2003), Modelling of seismic waves in heterogeneous media using a wavelet-based method: Application to fault and subduction zones, *Geophys. J. Int.*, *154*, 483–498.

Hong, T.-K., and J. Xie (2005), Phase composition of regional waves from underground nuclear explosions, *J. Geophys. Res.*, *110*, B12302, doi:10.1029/2005JB003753.

Jo, N. (2007), Numerical simulation of ground motion caused by fault rupture, Ph.D. thesis, 103 pp., Seoul Natl. Univ., Seoul.

Kennett, B. L. N. (1986), *Lg* waves and structural boundaries, *Bull. Seismol. Soc. Am.*, *76*, 1133–1141.

Kennett, B. L. N., and T. Furumura (2001), Regional phases in continental and oceanic environments, *Geophys. J. Int.*, *146*, 562–568.

Kim, W.-Y. (1998), The M_L scale in eastern North America, *Bull. Seismol. Soc. Am.*, *88*, 935–951.

Korea Institute of Nuclear Safety (2007), White paper on nuclear safety 2007 (in Korean), *Publ. 11-1350000-001105-10*, Minist. of Sci. and Technol., Korea Inst. of Nucl. Safety, Daejeon, South Korea.

Massé, R. P. (1981), Review of seismic source models for underground nuclear explosions, *Bull. Seismol. Soc. Am.*, *71*, 1249–1268.

Nuttli, O. W. (1973), Seismic wave attenuation and magnitude relations for eastern North America, *J. Geophys. Res.*, *78*(5), 876–885.

Nuttli, O. W. (1981), On the attenuation of *Lg* waves in western and central Asia and their use as a discriminant between earthquakes and explosions, *Bull. Seismol. Soc. Am.*, *71*, 249–261.

Patton, H. J. (2001), Regional magnitude scaling, transportability, and M_S:*mb* discrimination at small magnitudes, *Pure Appl. Geophys.*, *158*, 1951–2015.

Patton, H. J., and S. R. Taylor (1995), Analysis of *Lg* spectral ratios from NTS explosions: Implications for the source mechanisms of spall and the generation of *Lg* waves, *Bull. Seismol. Soc. Am.*, *85*, 220–236.

Sagong, H., C.-S. Cheong, and S.-T. Kwon (2003), Paleoproterozoic orogeny in South Korea: Evidence from Sm-Nd and Pb step-leaching garnet ages of Precambrian basement rocks, *Precambrian Res.*, *122*, 275–295.

Sato, H., and M. Fehler (1998), *Wave Propagation and Scattering in the Heterogeneous Earth*, Springer, New York.

Sheen, D.-H., K. Tuncay, C.-E. Baag, and P. J. Ortoleva (2006), Parallel implementation of a velocity-stress staggered-grid finite-difference method for 2-D poroelastic wave propagation, *Comput. Geosci.*, *32*, 1182–1191.

Shih, X. R., K.-Y. Chun, and T. Zhu (1994), Attenuation of 1–6 *s Lg* waves in Eurasia, *J. Geophys. Res.*, *99*(B12), 23,859–23,874.

Taylor, S. (1996), Analysis of high-frequency *Pg/Lg* ratios from NTS explosions and western U.S. earthquakes, *Bull. Seismol. Soc. Am.*, *86*, 1042–1053.

Vidale, J., D. V. Helmberger, and R. W. Clayton (1985), Finite-difference seismograms for *SH* waves, *Bull. Seismol. Soc. Am.*, *75*, 1765–1782.

Wallace, T., D. Helmberger, and G. Engen (1985), Evidence for tectonic release from underground nuclear explosions in long-period *S* waves, *Bull. Seismol. Soc. Am.*, *75*, 157–174.

Walter, W. R., K. Mayeda, and H. J. Patton (1995), Phase and spectral ratio discrimination between NTS earthquakes and explosions. Part 1: Empirical observations, *Bull. Seismol. Soc. Am.*, *85*, 1050–1067.

Xie, J., and H. J. Patton (1999), Regional phase excitation and propagation in the Lop Nor region of central Asia and implications for *P/Lg* discriminants, *J. Geophys. Res.*, *104*(B1), 941–954.

Xie, X.-B., and T. Lay (1994), The excitation of *Lg* waves by explosions: A finite-difference investigation, *Bull. Seismol. Soc. Am.*, *84*, 324–342.

Yoshimoto, K., H. Sato, and M. Ohtake (1993), Frequency-dependent attenuation of *P* and *S* waves in the Kanto area, Japan, based on the coda-normalization method, *Geophys. J. Int.*, *114*, 165–174.

Yu, S. H. (2006), Development of gravity model and Moho discontinuity in the Korean Peninsula and its surrounding seas using GRACE geopotential data (in Korean), Ph.D. thesis, p. 102, Yonsei Univ., Seoul.

Zhang, T.-R., and T. Lay (1995), Why the *Lg* phase does not traverse oceanic crust, *Bull. Seismol. Soc. Am.*, *85*, 1665–1678.

Zhou, R.-M., B. W. Stump, and C. T. Hayward (2006), M_S:m_b discrimination study of mining explosions in Wyoming, USA, and in QianAn, China, *Bull. Seismol. Soc. Am.*, *96*, 1742–1752.

C.-E. Baag, School of Earth and Environmental Sciences, Seoul National University, Shinlim-dong, Kwanak-gu, Seoul 151-742, South Korea.

H. Choi, Korea Institute of Nuclear Safety, P.O. Box 114, Yuseong-gu, Daejeon 305-600, South Korea.

T.-K. Hong, Department of Earth System Sciences, Yonsei University, Shinchon-dong, 134, Seodaemun-gu, Seoul 120-749, South Korea. (tkhong@yonsei.ac.kr)

D.-H. Sheen, Korea Institute of Geoscience and Mineral Resources, Daejeon 305-350, South Korea.